Influence of fluid properties on bubble formation, detachment, rising and collapse; Investigation using volume of fluid method

Peyman Zahedi*,†, Reza Saleh*, Roberto Moreno-Atanasio**, and Kianoosh Yousefi*

*Department of Mechanical Engineering, Mashhad Branch, Islamic Azad University, Mashhad, Iran
**Faculty of Engineering and Built Environment, The University of Newcastle, Australia

Abstract–Numerical simulations have been carried out to investigate the formation and motion of single bubble in liquids using volume-of-fluid (VOF) method using the software platform of FLUENT 6.3. Transient conservation mass and momentum equations with considering the effects of surface tension and gravitational force were solved by the pressure implicit splitting operator (PISO) algorithm to simulate the behavior of gas–liquid interface movements in the VOF method. The simulation results of bubble formation and characteristics were in reasonable agreement with experimental observations and available literature results. Effects of fluid physical properties, operation conditions such as orifice diameter on bubble behavior, detachment time, bubble formation frequency and bubble diameter were numerically studied. The simulations showed that bubble size and bubble detachment times are linear functions of surface tension and decrease exponentially with the increase in liquid density. In contrast, only a small influence of the fluid viscosity on bubble size and detachment time was observed. Bubble collapse at a free surface simulation with VOF method was also investigated.

Keywords: Bubble, Simulation, Two Phase Flow, Volume of Fluid

INTRODUCTION

Flows with a spatial variation of fluid properties due to density variation, such as gas-liquid interfaces, can be found in many engineering and environmental applications. Bubble columns are intensively used as multiphase contactors and reactors in chemical, biochemical and petrochemical industries. They provide several advantages during operation and maintenance such as high heat and mass transfer rates, compactness and low operating and maintenance costs [1]. Many investigations in this discipline focus on subjects such as bubble characteristics, local and average heat transfer measurements, studies of flow regimes and computational fluid dynamics, and mass transfer studies [2-11]. Although a tremendous number of studies exist in the literature, bubble columns are still not well understood because most of these studies are often oriented on only one phase, i.e., either liquid or gas. However, the main point of interest should be the study of the interaction between the different phases, which are in fact intimately linked. Single bubble behavior plays an important role in determining the flow, mass and heat transfer characteristics in the bubble columns and fluidized beds, since its generation and rise can stir up the liquid and intensify the interphase disturbance. This disturbance makes sufficient inter-phase contact and efficiency improvement of mass and heat transfer in the reactors [12].

In the past several decades a number of different methods have been developed to simulate complex two-phase flow problems. There are three basic approaches commonly employed in CFD for the study of multiphase flows: Eulerian-Eulerian (E-E) method, Eulerian-Lagrangian (E-L) method and direct numerical simulation (DNS) method [13-15]. The DNS approach is often chosen to study the behavior of formation and rising bubble in bubble columns.

To solve the moving interface problem, there are various methods to predict the phase interface position and motion in DNS method such as the fixed-grid method which is frequently used due to its efficiency and relative ease in programming. The numerical techniques used to solve the moving interface problem with fixed, regular grids are improved as the front capturing method. In the front capturing method a moving interface is implicitly represented by a scalar-indicator function defined on a fixed, regular mesh point. Among the techniques of front capturing, the volume of fluid (VOF) method is designed for two or more immiscible fluids where the position of the interface between the fluids is of interest.

VOF, originally developed by Hirt and Nichols [16], has been the most widely used approach to simulate free-surface flows. It has also received a considerable amount of attention in the study of phase change phenomena. An improved VOF method with phase change has also been used to simulate two-dimensional film boiling and to predict liquid evaporation rates [17-19]. Droplet impacting on hot surfaces [20,21] and the evaporation of droplets on hot surfaces [22,23] are also simulated by VOF method.

The VOF method can also be used to accurately predict the shape of the interface between the fluids. However, no boundary condition of interface slip is specified in the VOF model; therefore, the gas and liquid phases share a common velocity field [24]. Sometimes, it is difficult to consider the interaction between two phases, which is the key to successfully describe the flow behavior. We have tried using the VOF model to analyze the performance of a single bubble rising in liquid. In this paper, the VOF method was adopted to simulate the 2D bubbling behavior formed from the single orifice

---

of small diameter (0.5-1.5 mm) at low constant gas flow inlet. Computational results have also been compared with experimental data. The effects of liquid density, liquid viscosity, surface tension, velocity of orifice gas and orifice size on the bubble behavior including the detachment time, average diameter and coalescence time of bubbles were systematically investigated by using computer simulations.

NUMERICAL SIMULATION

1. Governing Equations

The CFD software FLUENT 6.3 was used to simulate the behavior of a single bubble in a stagnant liquid. The simulations were performed in two-dimensional domains. The VOF model was used, which allows the construction of the interface to become part of the solution based on the same grid system. The volume and pressure variation of the gas chamber in the bubble formation are relative small. Hence the gas is treated as an incompressible phase. Continuity the mass and momentum equation for the two-phase flow are represented as:

$$\nabla \cdot \vec{u} = 0 \tag{1}$$

$$\frac{\partial(\rho\vec{u})}{\partial t} + \nabla \cdot (\rho\vec{u}\vec{u}) = -\nabla p + \nabla \cdot \{\mu[\nabla\vec{u} + (\nabla\vec{u})^T]\} + F_s + \rho\vec{g} \tag{2}$$

where $\vec{u}$ is the velocity vector, p is the scalar pressure, μ is the liquid viscosity and F_s stands for a surface tension source term.

The VOF method has less computational complexity, higher precision, and is easier to realize in comparison to other methods. The basis of the VOF method is the fractional volume of fluid scheme for tracking free boundaries. A function F(x, y, t) is defined whose value is unity at any point occupied by fluid and zero elsewhere. When averaged over the cells of a computational mesh, the average value of F in a cell is equal to the fractional volume of the cell occupied by fluid. In particular, a unit value of F corresponds to a cell full of fluid, whereas a zero value indicates that the cell contains no fluid. Cells with F values between zero and one contain a free surface. Since the indicator function is not explicitly associated with a particular front grid, an algorithm is needed to reconstruct the interface [16]. An interface exists in those cells that give a volume of fluid value of neither 0 nor 1. Thus, the fluid volume functions in every unit are given as:

$$F = \frac{\text{volume of fluid in unit}}{\text{volume of unit}} \tag{3}$$

$$F = \begin{cases} 0 & \text{in bubbles} \\ 0 < F < 0 & \text{interface} \\ 1 & \text{in liquid fluid} \end{cases} \tag{4}$$

The method of tracing interface boundary is achieved by solving the volume fraction continuity equation of one or several phases. The transport equation of fluid volume function is:

$$\frac{\partial F}{\partial t} + u\frac{\partial F}{\partial x} + v\frac{\partial F}{\partial y} = 0 \tag{5}$$

Methods based on the VOF approach automatically guarantee the conservation of the mass of liquid. The key success of the VOF approach is the appropriate evaluation of the fluxes across the cell faces

in predicting the shape of the interface.

2. Interface Reconstruction Techniques

There are several methods for solving fluid volume functions, including the donor-acceptor method [16], flux line-segment model for advection and interface reconstruction (FLAIR) method [25], simple line interface calculation (SLIC) method and piecewise linear interface calculation (PLIC) method [26]. The PLIC method takes transport among adjacent interface fluid into consideration in full detail, and the reconstruction results are comparatively precise. Therefore, the PLIC method was adopted here to conduct interface reconstruction. The geometric reconstruction based on the piecewise linear interface construction (PLIC) method by Youngs [26] assumes that the interface between two fluids has a linear slope within each cell and uses this linear profile for the calculation of the advection of fluid through the cell faces. The position of the linear interface relative to the center of each partially filled interface based on the information about the volume fraction and its derivatives in the cell is initially determined. The amount of fluid that is advected through each face is calculated using the computed linear interface representation and information about the normal and tangential velocity distribution on the cell face and the volume fraction in each cell is ascertained using the balance fluxes calculated during the previous step.

The mixed fluid properties density and viscosity are weighted by the volume fractions and of the two fluids:

$$\rho = F_1\rho_1 + [1 - F_1]\rho_2 \tag{6}$$

$$\mu = F_1\mu_1 + [1 - F_1]\mu_2 \tag{7}$$

Surface tension in the interface is introduced in the model by the continuum surface force (CSF) model [27]. Only the forces normal to the interface are considered and the surface tension force is considered to be constant along the surface. The surface tension σ is changed into a volume force in the momentum equation according to the divergence theorem. This volume force for gas and liquid two-phase is given by:

$$F_s = \sigma\frac{\rho k\nabla F_l}{0.5(\rho_g + \rho_l)} \tag{8}$$

where $k = \nabla \cdot \hat{n}$, $\hat{n} = n/|n|$, $n = \nabla F_q$.

The transport equation of each volume fraction F_1 and F_2 in an incompressible two-fluid system is given by

$$\frac{\partial F_i}{\partial t} + \nabla \cdot (\vec{u}_i F_i) = 0, \quad i = 1, 2 \tag{9}$$

with u_i being the velocity of the component i.

It is sufficient to consider the transport equation of the volume fraction F_1 only, which this approach is called surface compression that corrects the fluxes near the interface between two phases [28]

$$\frac{\partial F_1}{\partial t} + \nabla \cdot (\vec{u}_1 F_1) = 0 \tag{10}$$

To solve this transport equation, the velocity $\vec{u}_1$ of fluid 1 is needed. In the widely used original VOF method, the velocity $\vec{u}_1$ is assumed to be equal to the mixed velocity $\vec{u} = \vec{u}_1$

$$\frac{\partial F_1}{\partial t} + \nabla \cdot (\vec{u} F_1) = 0 \tag{11}$$

In various applications of multi-phase flows, a fundamental understanding of the physics for the case of a bubble rising and deforming in a quiescent viscous liquid is essential. Herein, the bubble shapes have a tendency to vary greatly, depending on where the bubbles lie within the different flow regimes. The bubble rising behaviors can usually be correlated against four non-dimensional parameters such as the Morton number which is defined as [24]:

$$Bo = \frac{g\rho^l D^2}{\sigma} \tag{12}$$

$$M = \frac{g(\mu^l)^4}{\rho^l \sigma^3} \tag{13}$$

The Froude number defined as [29]:

$$Fr = \frac{U_o^2}{gd_o} \tag{14}$$

and the Reynolds number defined as:

$$Re = \frac{\rho^l UD}{\mu^l} \tag{15}$$

where, D and d_o represent the diameter of the bubble and the orifice diameter, respectively. The Bond number represents the contribution of the effects of surface tension and buoyancy, whereas the Morton number, which is sometimes referred to as the property group, measures the relative importance of viscous and surface tension forces. Following similar definition, the Reynolds number signifies the contribution between the inertia and viscous effects. Note that most
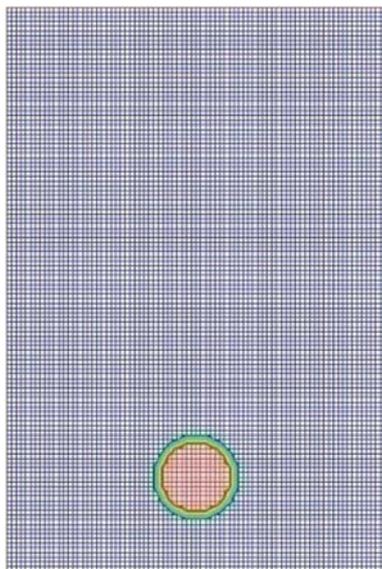
experimental results on bubble rising in liquid are presented using the Reynolds number based on the measured bubble terminal rising velocity (U_∞), which is given by $Re_{exp} = \rho^l DU_\infty/\mu^l$.

3. Solution Method, Mesh Dependency and Model Geometry

To find the dependency of the simulation results on the mesh size, a cylindrical bubble column with 20 mm width and 30 mm height was simulated in Cartesian coordinate system as shown in Fig. 1. Initially, a static bubble with 4 mm diameter was released and allowed to rise in the stagnant liquid. The model geometry was built and meshed using GAMBIT and then imported into FLUENT for flow calculations. For the purpose of finding how many computational cells on the solution domain were required to solve the continuity, momentum and volume of fluid function equations, five different mesh sizes were considered. The grid sizes were 0.2 mm×0.2 mm, 0.25 mm×0.25 mm, 0.3 mm×0.3 mm, 0.35 mm×0.35 mm, 0.4 mm× 0.4 mm, and the corresponding numbers of grid points were 3825, 4902, 6700, 9600, 15150, respectively. The time step was set as 0.0001 s.

The finite volume method implicit iteration was used to solve the continuity, momentum and volume of fluid function equations. The first-order upwind scheme was applied to the discretization of the flow equations. This scheme is more stable than the second-order upwind scheme and is used most often with reasonable accuracy [12]. The pressure-velocity coupling was carried out using the pressure-implicit with splitting of operators (PISO) method pressure discretization method was pressure staggering option (PRESTO).

The numerical simulations were executed on the software platform of Fluent 6.3 running on a high performance 24-core super computer. The solution area made with 9600 cells (mesh size 0.25 mm) and the initial position of the released bubble are shown in Fig. 1. The simulation results for the rising of the single bubble at three different time steps are shown in Fig. 2. In Fig. 2 blue and red represent the liquid and gas phases, respectively. The profiles of the single bubble rising with different grid sizes at time of 0.05 s are shown in Fig. 3 (the color coding is similar to that of Fig. 2). These simulation results at time 0.05 s were considered and evalu-

Fig. 1. The solution area of rising single bubble and initial released bubble made with 9600 meshes (mesh size 0.25 mm).
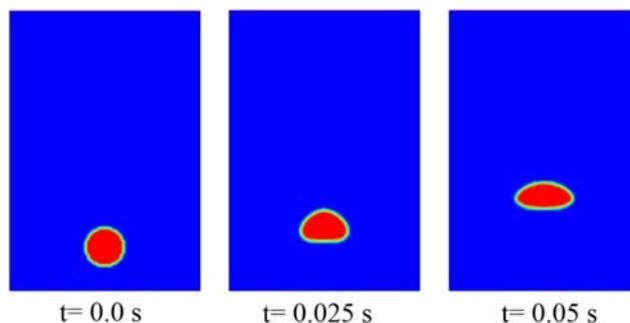
Fig. 2. Simulation results of single bubble with 4 mm diameter rising at three different time steps with 9600 meshes.
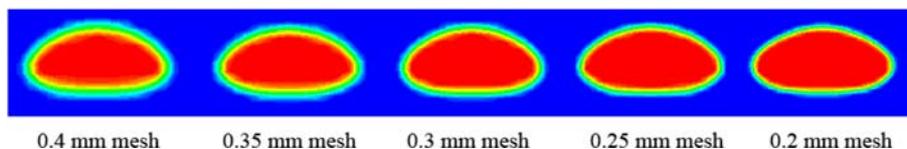
Fig. 3. The profiles of single bubble rising with different grid sizes at time of 0.05 s.

Contours of Y Velocity (mixture) (m/s) (Time=5.0000e-02)
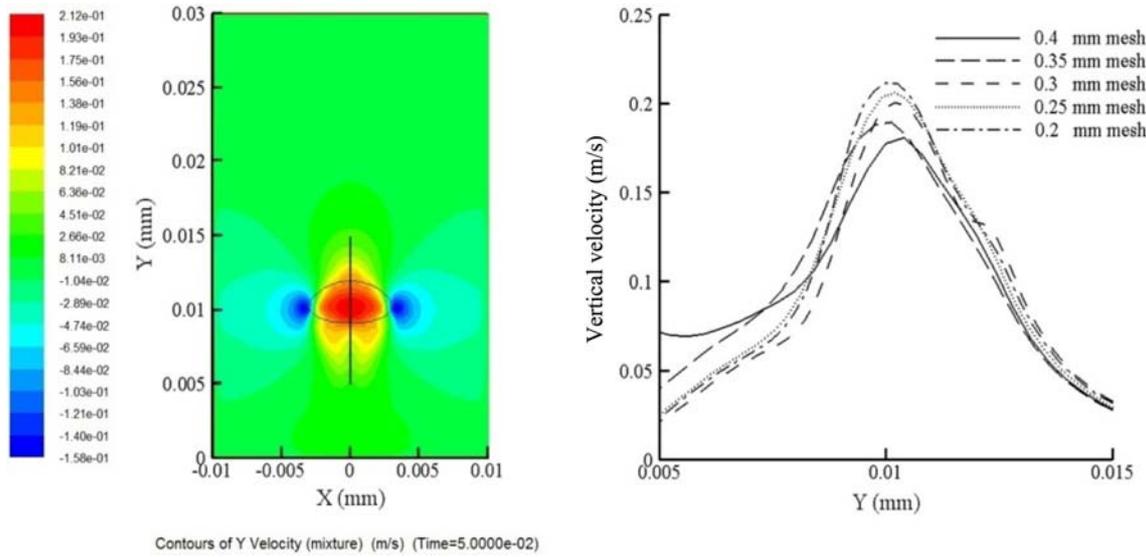
Fig. 4. Contour and the plot of vertical velocities at y direction on the center line (x=0, 0.005 mm≤y≤0.015 mm) with various meshes at t=0.05 s.
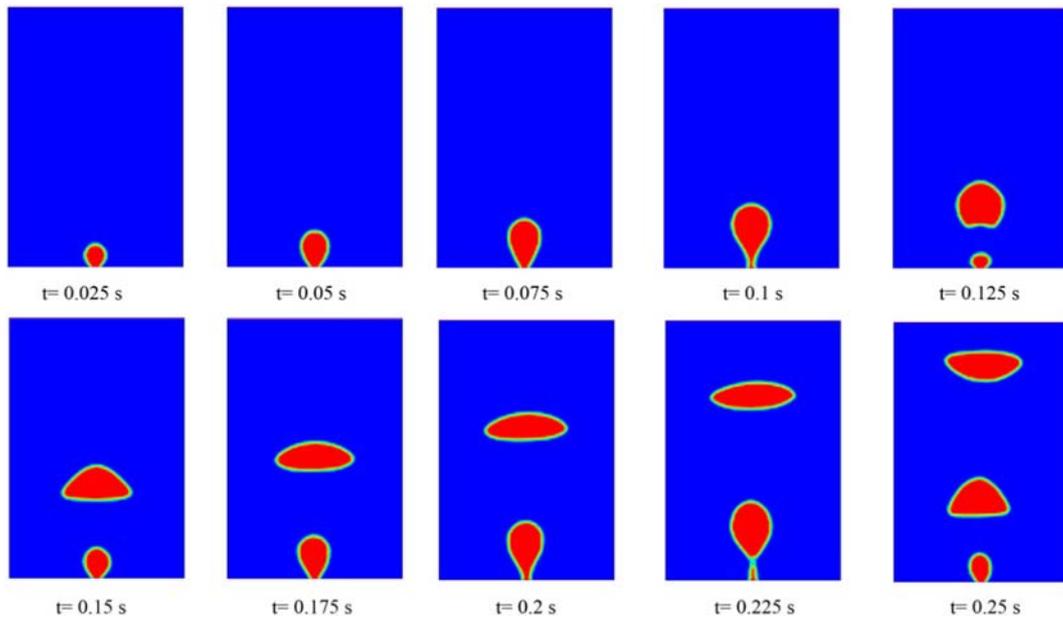
Fig. 5. Simulations of bubble formation from an orifice when d_o=1 mm and V_g=0.2 m/s with 0.25 mm mesh size.

ated; therefore, the contour and the plot of vertical velocities at y direction on the center line (x=0, 0.005 mm≤y≤0.015 mm) with all different meshes was plotted and shown in Fig. 4.

The effect of mesh size on simulation results was also examined by simulating the formation and rising of a bubble with different mesh sizes for the cases in which the orifice diameter was 0.2 and 1 mm. Fig. 5 shows the formation and detachment with 0.25 mm mesh size. The bubble generation includes two stages: expansion and detachment. During the first stage the gas bubble expands and grows larger while still in contact with the mouth of the orifice (Fig. 5 until t=0.1 s). Surface tension force plays a key role in the bubble expansion. As the bubble grows larger, the bubble keeps rising, and forms a slender neck which connects the body of the bubble with

the orifice (t=0.1 s). When the buoyancy is greater than the liquid drag force on the bubble, the bubble detaches from the orifice and moves up (Fig. 5 at t=0.125 s), during which the bubble keeps deforming. After that another bubble is generated, following by expansion, growth, and detachment.

Fig. 6 shows the profiles of formed bubbles with different meshes when the gas velocity was 0.2 m/s at time of 0.25 s. Vertical velocities of the first formed bubble with different computing meshes are plotted in Fig. 7 and contour and velocity vectors of vertical velocities at t=0.25 s with 0.25 mesh size are shown in Fig. 8(a) and (b), respectively. It is noticeable that there is a peak indicated in Fig. 7 at 0.1-0.15 s time bracket and it is related to the detachment time which is associated with an initial increase in velocity which is fol-
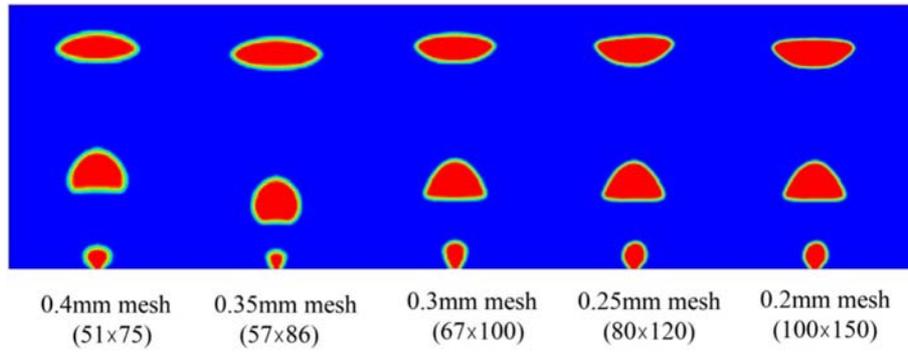
Fig. 6. Bubble profiles with different computing meshes when v_g=0.2 m/s at time of 0.25 s.
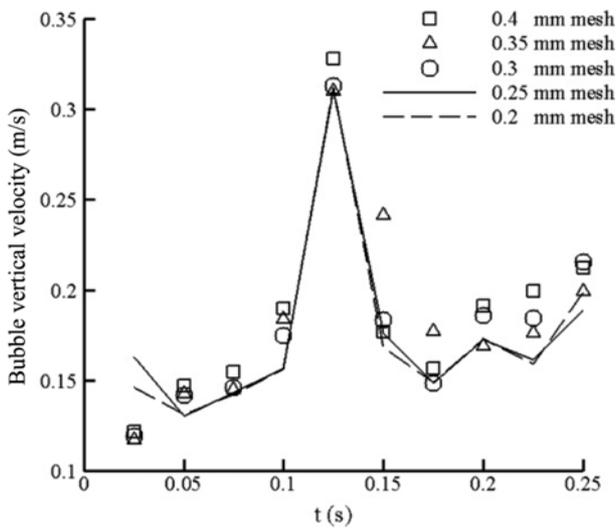
Fig. 7. The first bubble Vertical velocity versus time with different meshes when v_g=0.2 m/s.

lowed by a decrease in bubble velocity.

To more deeply analyze the mesh dependency the aspect ratio,

E, of the bubble was calculated according to the expression:

$$E = \frac{d_v}{d_h} \tag{16}$$

where, d_v and d_h are the vertical and horizontal diameters, respectively; this ratio for the first formed bubble with different meshes is plotted in Fig. 9. From Figs. 6-8, the values of simulated size aspect ratio with 0.25 mm, 0.2 mm grid sizes are very close. Similar trends were found in the profiles of bubbles at different grid sizes. The bubble profiles during the bubble growth with 0.25 mm and 0.2 mm mesh sizes provided in Fig. 6 were approximately the same. These results indicate that the simulations are grid independent for the mesh sizes studied here and that reasonable accuracy can be reached with a mesh size of 0.25 mm in this 2D simulation. Based on this consideration and the computational time a the grid size of 0.25 mm was chosen in the 2D simulations. Of course, the mesh size can be reduced further but the computational time will increase dramatically.

4. Simulation Verification

The experimental set up used to investigate the bubble formation under constant flow conditions is shown in Fig. 10. A glass column with a square cross section (with each side of 10 cm) and
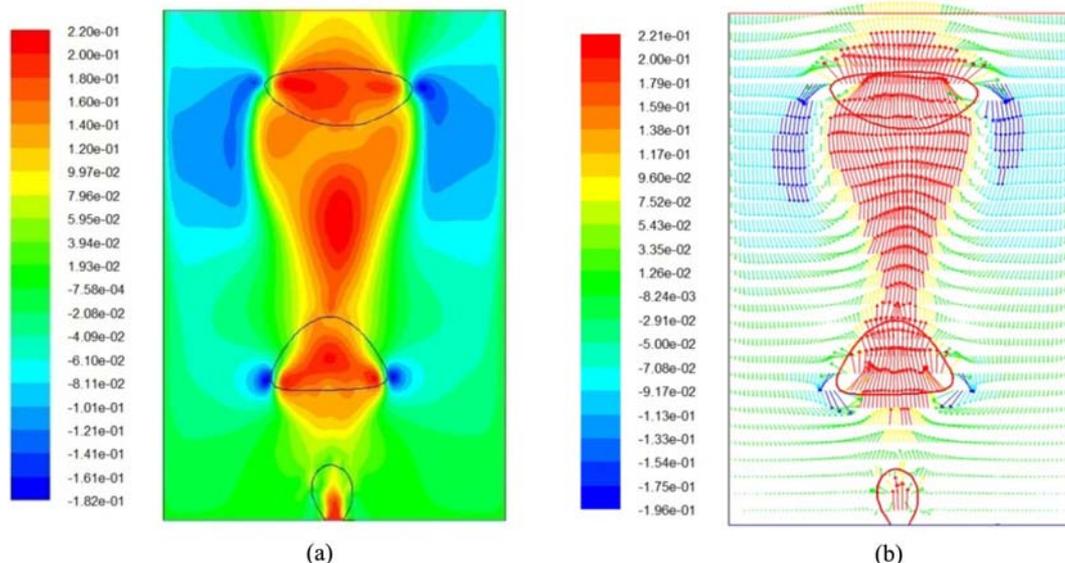
Fig. 8. Contours (a) and vector (b) of vertical velocities at t=0.25 s with 0.25 mesh size.
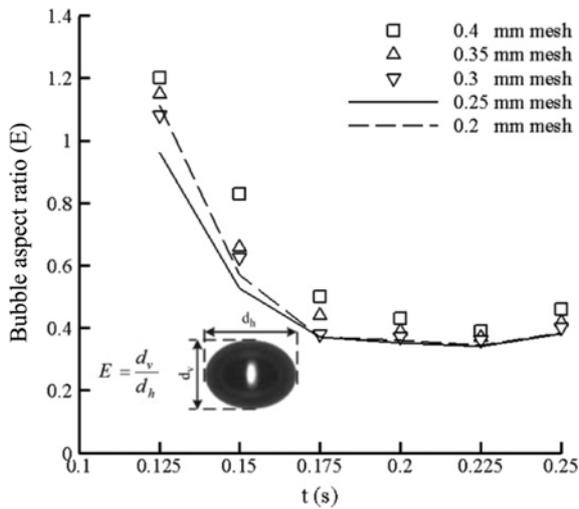
Fig. 9. Aspect ratio (E) with different meshes plotted against time.
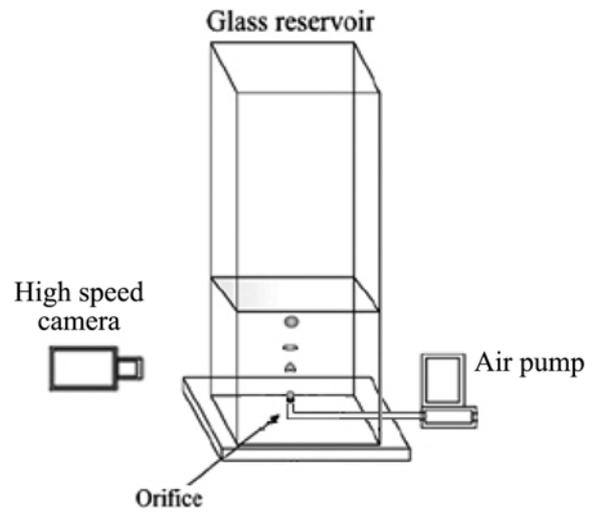
Fig. 10. Schematic diagram of the experimental set-up.
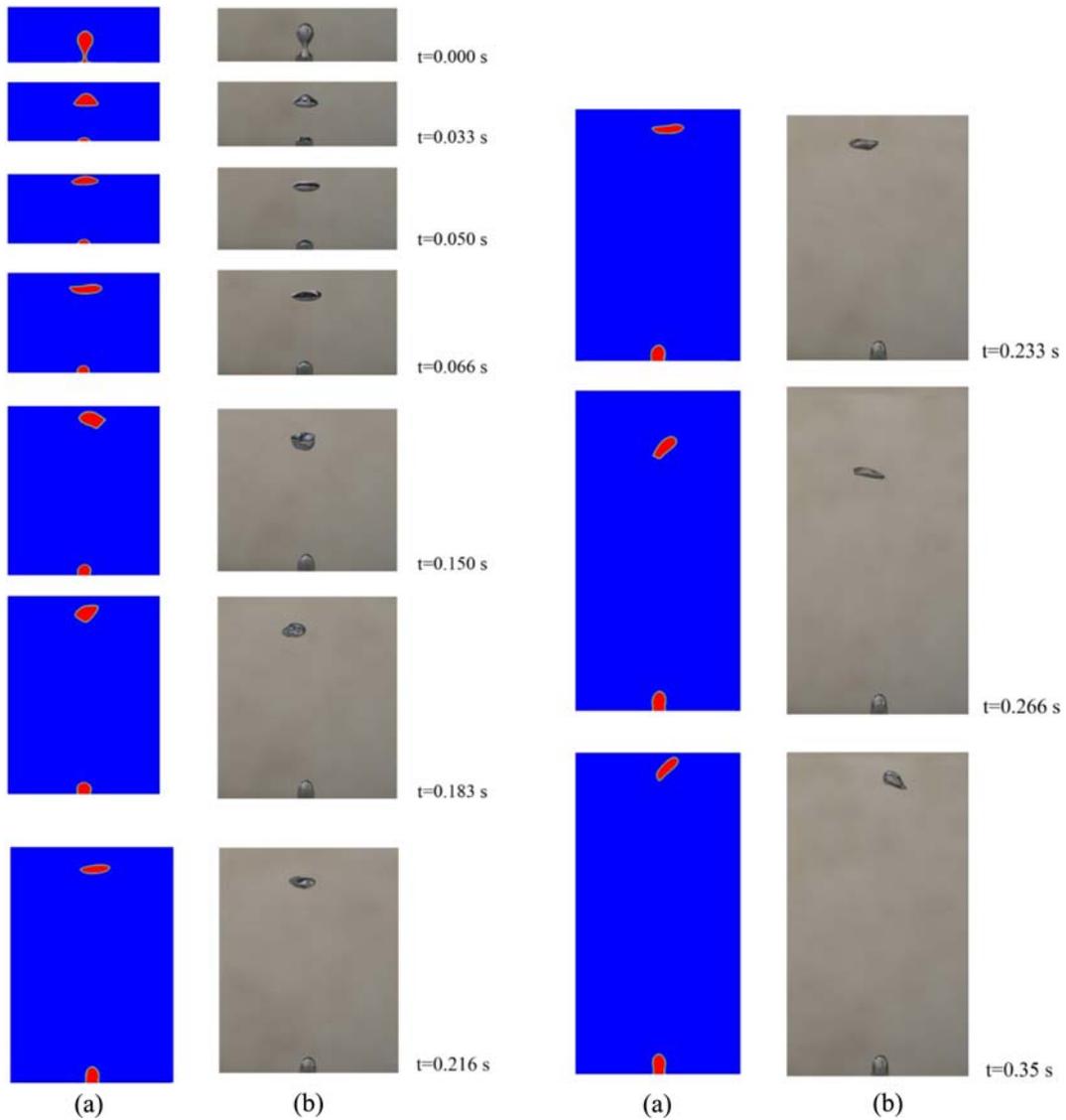
Fig. 11. Comparisons of simulations and experiments of bubble formation and rising motion from an orifice of 4.5 mm diameter with constant flow rate of 2.5e-7 m³/s (a) simulations and (b) experiments.

Table 1. Comparisons of calculated and measured bubble velocities in numerical and experimental method

	Bubble velocity (m/s)
Experimental method	0.224
Numerical simulation	0.245
Relative error (%)	9

with a height of 50 cm was used. In experiments, water was used as the liquid phase, with the static liquid level maintained at 10 cm from the bottom of the column. Air was introduced in the column through the orifice with 4.5 mm diameter as shown in Fig. 10. The air flow rate was constant at 2.5e-7 m³/s using an air pump with flow controller. A high-speed digital camera (speed of 60 frames/s) recorded the bubble formation process. The bubble formation periods were characterized by analyzing the recorded movie files with snapshots taken every 0.016 s.

Comparisons between simulations and experiments of bubble formation and rising motion from orifice with air flow rate of 2.5e-7 m³/s and stagnant liquid are shown in Fig. 11. In addition, rise
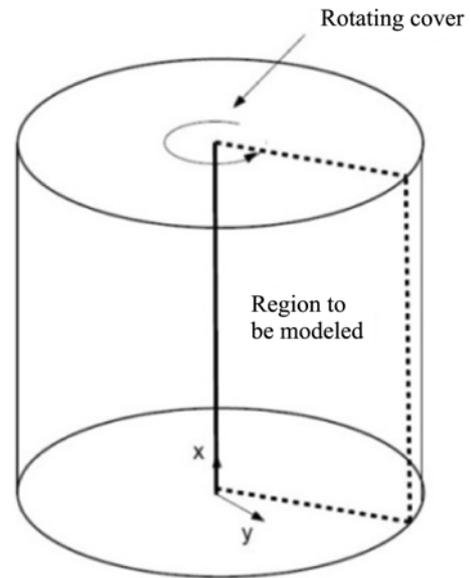
Fig. 12. Example of modeled region with axisymmetric boundary condition.
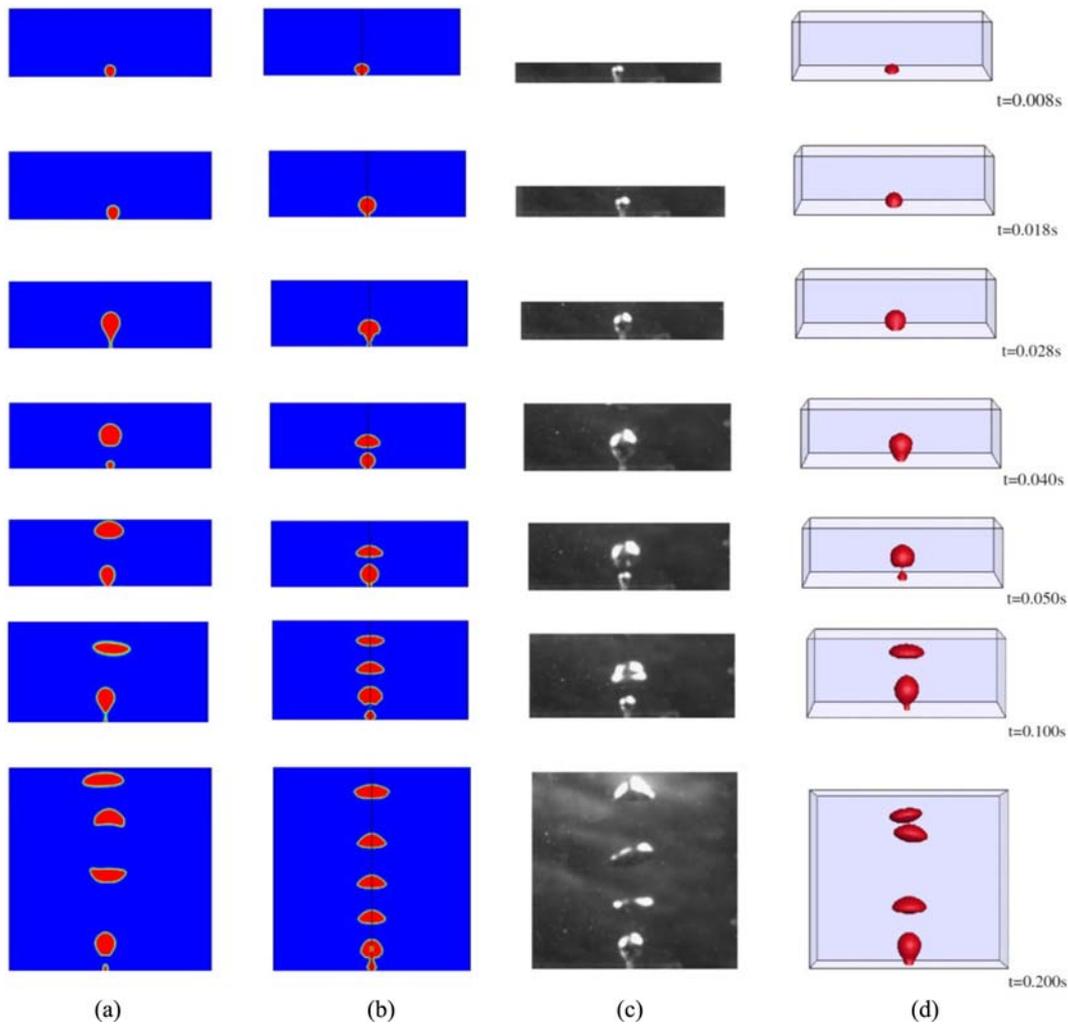
Fig. 13. Comparisons of experiments and simulations of bubble formation from an orifice of 1.0 mm diameter and rising motion when v_g=3 m/s (a) 2D simulation without axisymmetric boundary condition, (b) 2D axisymmetric simulation, (c) Experiments [30] and (d) 3D simulations [30].

velocities both in numerical simulations and experiments are listed in Table 1. The time of releasing the first bubble from orifice is considered as the starting time of experiment. The comparisons of bubble rise velocity between simulated results and those calculated from the experiments indicate that the agreement is good with a relative error of approximately 9% (Fig. 11). However, the behavior of 2D bubbles obtained from the numerical simulation is different to some extent from that of the bubbles measured in the experiment. Moreover the experiment of bubble formation was done under approximate constant gas flow rate while the simulation was carried out at strict condition of constant gas flow rate.

5. Axisymmetric Simulation

The assumption of axisymmetry implies that there are no circumferential gradients in the flow, but that there may be non-zero circumferential velocities. Examples of axisymmetric flow are in Fig. 12.

Yujie et al. [30] conducted a research based on two-dimensional numerical studies on single bubbling behavior. Three-dimensional numerical simulations on bubble formation in bubble columns were also investigated using the volume of fluid (VOF) model using Fluent 6.3, and the results were validated with the experimental observations. In the present research, 2D axisymmetric simulations in Cartesian coordinate system and without axisymmetric boundary condition were carried out and the results were compared with the experimental and 3D numerical simulation results by Yujie et al. [30].

Comparisons between simulations and experiments of bubble formation and rising motion from an orifice with 1 mm diameter and a high orifice gas velocity of 3.0 m/s in the experimental method [30], 2D axisymmetric simulations and without axisymmetric boundary condition are shown in Fig. 13. The physical characteristics of gas and liquid phases in the simulations are listed in Table 2. Bubble diameter and rise velocity are also listed in Table 3. It is found from Fig. 13 and Table 3 that axisymmetric simulations have a high relative error in comparison with 3D simulation and simulations without axisymmetric boundary condition. In axisymmetric simulation, bubble velocity and bubble diameter showed 37% and 18% relative error, respectively, compared with experiments. In axisymmetric simulation, bubble motion was incorrectly rising just in center

Table 2. Properties of gas and liquid phases in the simulations

ρ_g (kg/m³)	ρ_l (kg/m³)	μ_g (pa·s)	μ_l (pa·s)	σ_l (N/m)	d_o (mm)
1.225	9.982e2	1.789e-5	1.0e-3	7.28e-2	1.0

Table 3. Comparisons between simulations and experiments of characteristic data of bubble behavior form an orifice with 1.0 mm diameter and v_g=3.0 m/s

	Bubble diameter (mm)	Bubble velocity (m/s)
Experiments[30]	7.00	0.275
3D simulation [30]	7.12	0.262
2D axisymmetric simulation	5.7	0.173
2D simulation without axisymmetric boundary condition	7.65	0.253
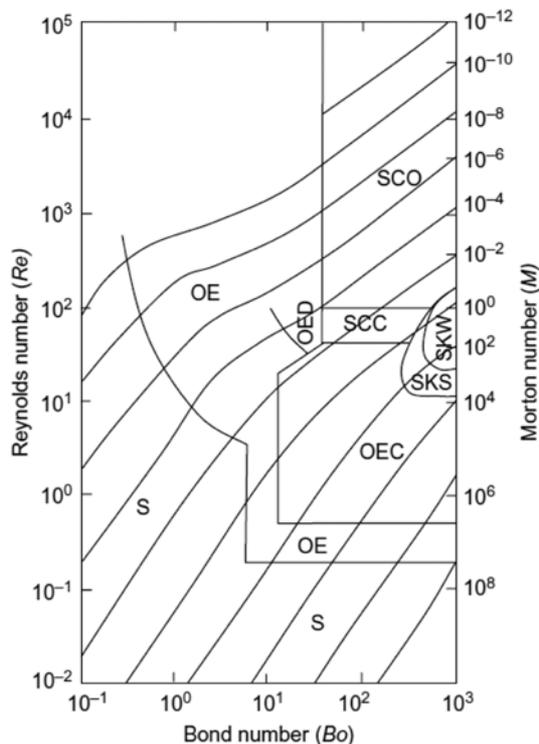
Fig. 14. Regime map of experimentally observed rising bubble shape according to Bhaga and Weber [31]: S-spherical, OE-oblate ellipsoid, OED-oblate ellipsoidal (disk-like and wobbling), OEC-oblate ellipsoidal cap, SCC-spherical cap with closed, steady wake, SCO-spherical cap with open, unsteady wake, SKS-skirted with smooth, steady skirt and SKW-skirted with wavy, unsteady skirt.

line of bubble column; however, in 2D simulation without axisymmetric boundary condition and in Cartesian coordinate system the bubble velocity and bubble diameter had 8% and 9% error, respectively. Indeed there is reasonable agreement between experiments and simulations of bubble behavior in the process of bubble generation and rising motion without axisymmetric boundary condition.

According to Bhaga and Weber [31], the shapes of a single rising bubble under a range of Reynolds and Bond numbers have been observed and reported, as shown in Fig. 14. In general, small bubbles that experience low Reynolds or Bond number rise in a steady manner and maintain spherical shape (Re<1 or Bo<1). At intermediate Reynolds and Bond numbers, the shapes of bubbles will be significantly affected by the flow conditions (1<Re<100 and 1<Bo<100). Bubble shapes such as oblate ellipsoid, disk-like, oblate ellipsoidal cap, skirt bubble and spherical-cap are observed. In spite of the difference in shapes, the bubbles maintain a straight path upwards in the liquid. At high Reynolds number (100<Re<500) the bubbles begin to deform into a toroidal shape in the high bond number regime (100<Bo<500), spherical-cap shape in the intermediate bond number regime (30<Bo<100) and oblate ellipsoid in the low Bond number regime (1<Bo<30). As the bubble size increases further, the onset of turbulent wake developing behind the bubbles becomes more prevalent, which subsequently leads to unsteady bubble motion. The bubbles may rise in a wobbly path, oscillate about a mean shape and could even coalesce or break up. When the Reynolds and Bond

numbers are not too high (Re<200 and Bo<200), the rising bubbles generally have axisymmetric shapes.

In most of the presented simulated cases in this study, for Bond numbers between 30 and 100 the predicted shapes agree well with the experiments as observed in Fig. 13. After detachment, the leading bubble takes the shape of a spherical cap with a strong wake (having high upward velocity at its center) behind it. This high-velocity jet in the center of the vortex behind the leading bubble forces its rear surface to move faster than the front surface of the bubble. This leads to merging of the front and rear surfaces of the leading bubble and results into the formation of a toroidal bubble. The previously formed large spherical cap bubble influences the growth of the second bubble significantly.

6. Influence of Liquid Surface Tension on Bubble behavior

There are many factors influencing the bubble behavior, including physical properties of the fluid such as surface tension, liquid density and viscosity. Fig. 15 shows volume fraction contours of simulation results of bubbling formation and rising process with varied liquid surface tension force for three different orifice diameters (0.5, 1 and 1.5 mm),when the constant gas mass flow is 1e-7 m^3/s. The simulation time for all cases in this simulation was 0.25 s. The effects of surface tension on bubble diameter and detachment time are shown in Figs. 16 and 17, respectively. From Fig. 16 there is an upward trend for the bubble diameter by increasing surface tension; moreover, detachment time saw a similar trend as shown in Fig. 17. However, bubble formation frequency is decreased. Surface tension increasing at constant orifice diameter and mass flow leads to reduction in bubble formation frequency, but bubble diameter and detachment time are increased. Detachment time delay makes more gas get into the growing bubble. Meanwhile, the increase of surface tension inhibits the bubble generation, which results in long average cycle and low frequency of bubble generation. Therefore, the average bubble diameter is relatively large. According to Eqs. (13) and (14), at constant Froude number and by decrease of Morton number caused by surface tension rise, bubble diameter and detachment time are increased.

7. Influence of Liquid Viscosity on Bubble behavior

The impact of liquid viscosity on bubble behavior was investi-
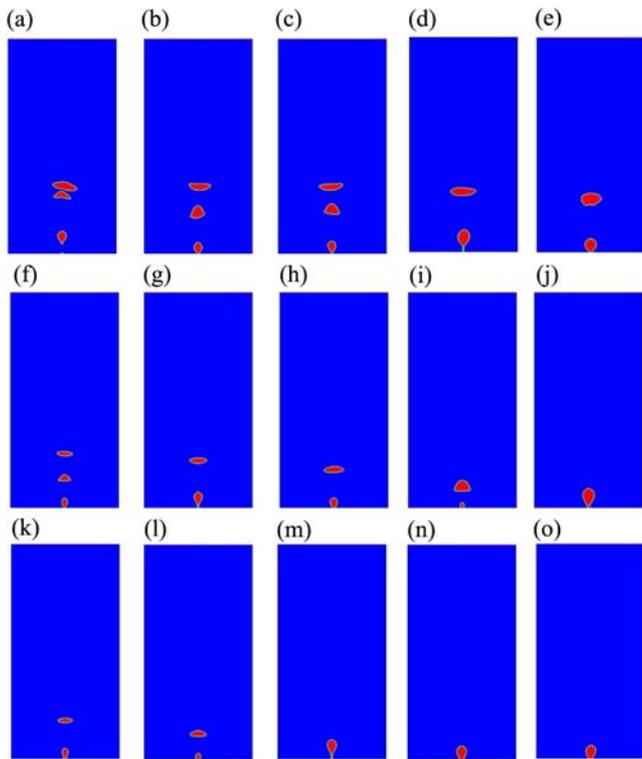
Fig. 15. Simulation results of bubble behavior under different surface tension forces at constant gas mass flow equals to 1e-7 m^3/s and t=0.25 s, (a, f, k) σ=0.0364 N/m, (b, g, l) σ= 0.0546 N/m, (c, h, m) σ=0.0728 N/m, (d, I, n) σ=0.1092 N/m, (e, j, o) σ=0.1456 N/m, (a-e) d_o=0.5 mm, (f-j) d_o=1 mm, (k-o) d_o=1.5 mm.
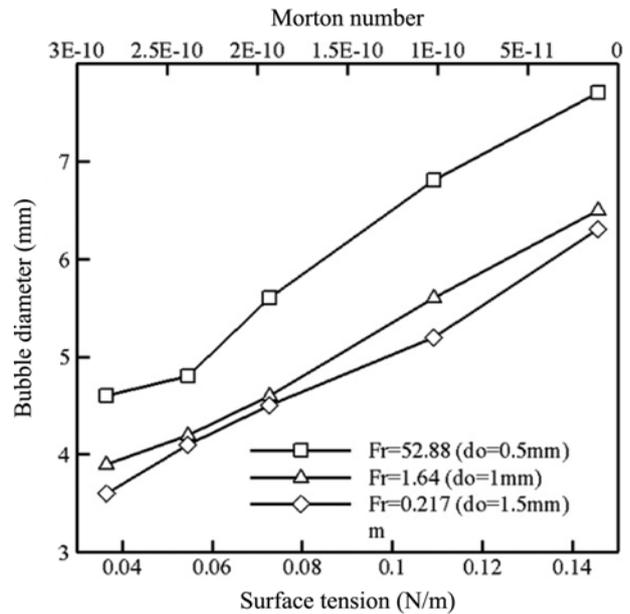
Fig. 16. Effects of surface tension on bubble diameter at constant gas mass flow equals to 1e-7 m^3/s and varied orifice diameter.
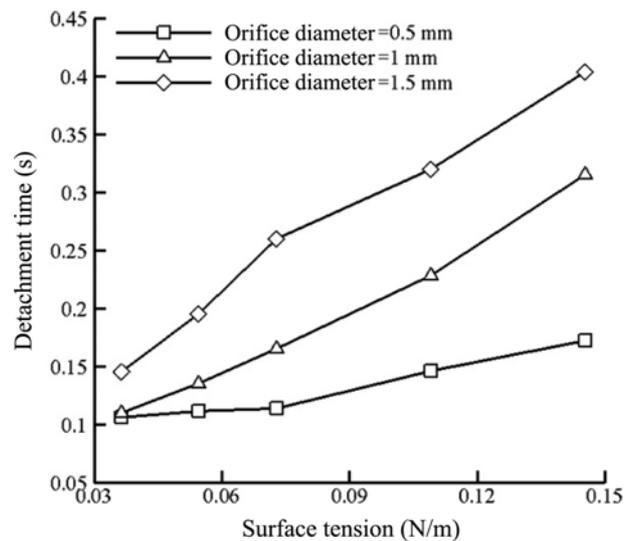
Fig. 17. Effects of surface tension on detachment time at constant gas mass flow equals to 1e-7 m^3/s and varied orifice diameter.

Table 4. Property parameters for studying the effect of liquid viscosity on bubble behavior

μ_l (kg/m·s)	ρ_l (kg/m³)	σ (N/m)	Morton number
1.003e-3	9.982e2	7.28e-2	2.57e-11
1.0e-2	9.982e2	7.28e-2	2.54e-7
2.0e-2	9.982e2	7.28e-2	4.07e-6
5.0e-2	9.982e2	7.28e-2	1.59e-4
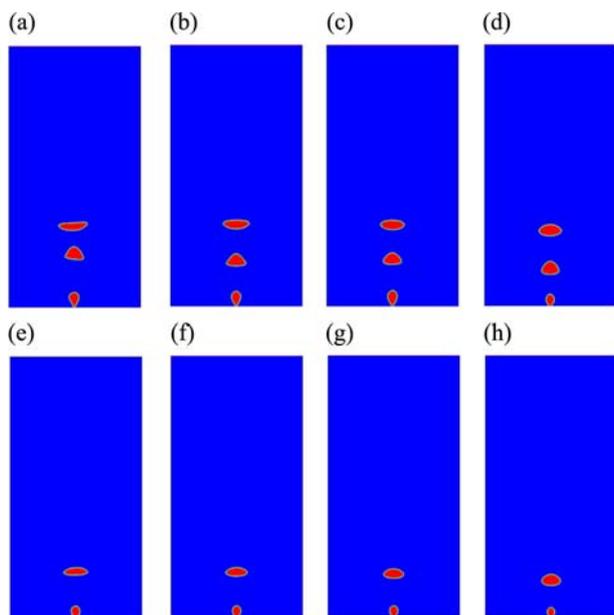
Fig. 18. Simulation results of bubble behavior under different liquid viscosity at constant gas mass flow equals to 1e-7 m³/s and t=0.25 s, (a-d) d_o=0.5 mm, (e-h) d_o=1 mm, (a, e) μ_l= 1.003e-3 kg/m·s, (b, f) μ_l=1.0e-2 kg/m·s, (c, g) μ_l=2.0e-2 kg/ m·s, (d, h) μ_l=5.0e-2 kg/m·s.

gated by liquids whose physical parameters are listed in Table 4. Simulation results at t=0.25 s and 1e-7 m³/s are shown in Fig. 18; as it is seen, no obvious change of bubbling behavior is found for varied liquid viscosity. Bubble diameter approximately stayed constant at varied liquid viscosity as it is shown in Fig. 19. The effect of liquid viscosity on detachment is given in Fig. 20. It is noticeable that bubble detachment time grew negligibly with the increase in liquid viscosity. However, these results indicate that the effect of liquid viscosity on bubbling behavior is not considerable at present simulations. It is worth noting that again, bubble formation frequency is reduced by increasing orifice diameter at constant mass flow.

8. Influence of Liquid Density on Bubble behavior

Density variation has a significant impact on bubble behavior, motion and rising. The physical parameters of the different liquid phases that have been used in order to investigate the density effects in bubble behavior are listed in Table 5. The simulated inlet gas is air with 1.225 kg/m³ density and 1.7894e-5 kg/m.s. The simulation results of bubbling behavior at two varied liquid density equal to 998.2 and 3,000 kg/m³ are shown in Fig. 21. It is evident that liquid density influences the bubble behavior remarkably. Comparing Fig. 21(j) with (e) one can find that increasing liquid density enhances
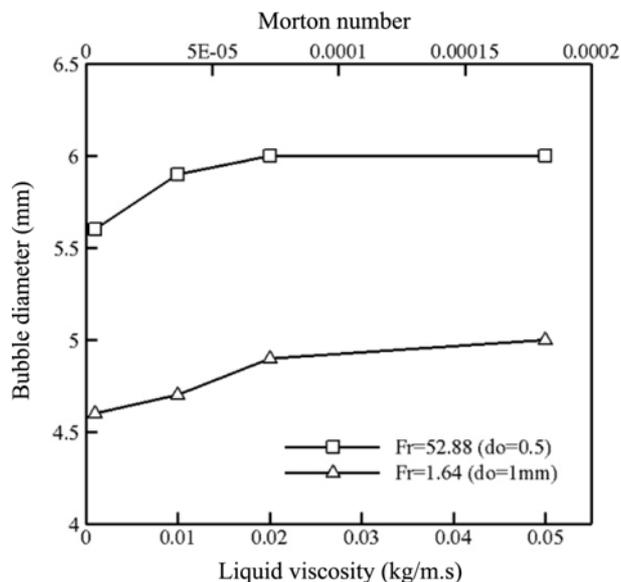
Fig. 19. Effects of liquid viscosity on bubble diameter at constant gas mass flow equals to 1e-7 m³/s and varied orifice diameter.
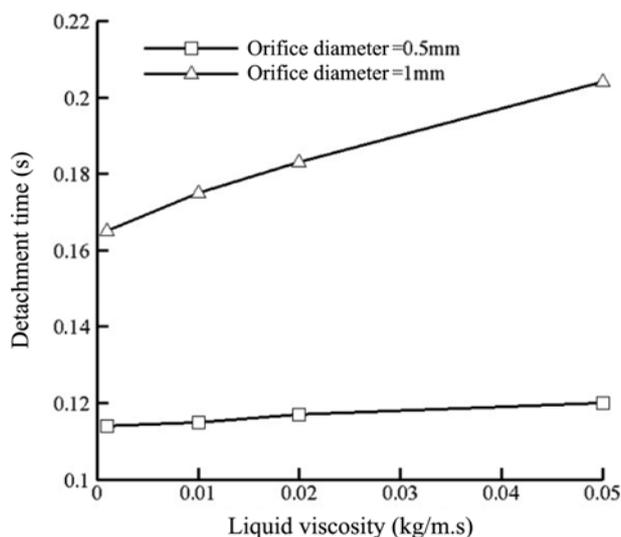
Fig. 20. Effects of liquid viscosity on detachment time at constant gas mass flow equals to 1e-7 m³/s and varied orifice diameter.

Table 5. Liquid characteristics used in investigating effects of liquid density on bubble behavior

ρ_l (kg/m3)	μ_l (kg/m·s)	σ (N/m)
500	1.003e-3	7.28e-2
998.2	1.003e-3	7.28e-2
1500	1.003e-3	7.28e-2
2000	1.003e-3	7.28e-2
3000	1.003e-3	7.28e-2

the frequency of single bubbling process because a fourth bubble can be found in Fig. 21(j) but only two bubbles can be found in Fig.
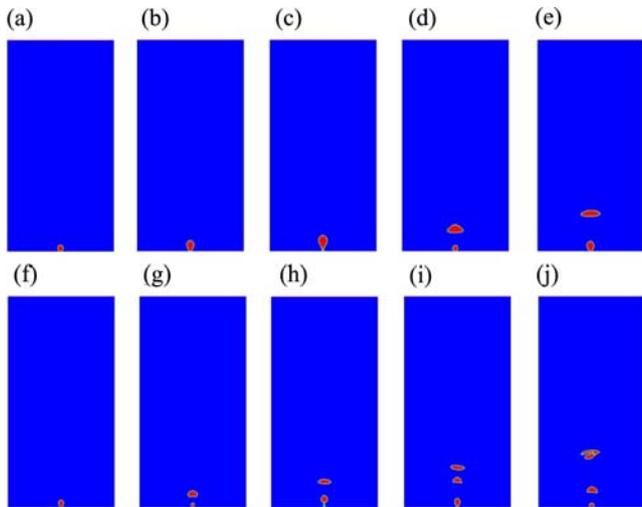
Fig. 21. Effects of liquid density on bubble behavior at constant mass flow equals to 1e-7 m³/s and d_o=1 mm, (a-e) ρ_l=998.2 kg/m³, (f-j) ρ_l=3,000 kg/m³, (a, f) t=0.05 s, (b, g) t=0.1 s, (c, h) t=0.15 s, (d, i) t=0.2 s, (e, j) t=0.25 s.
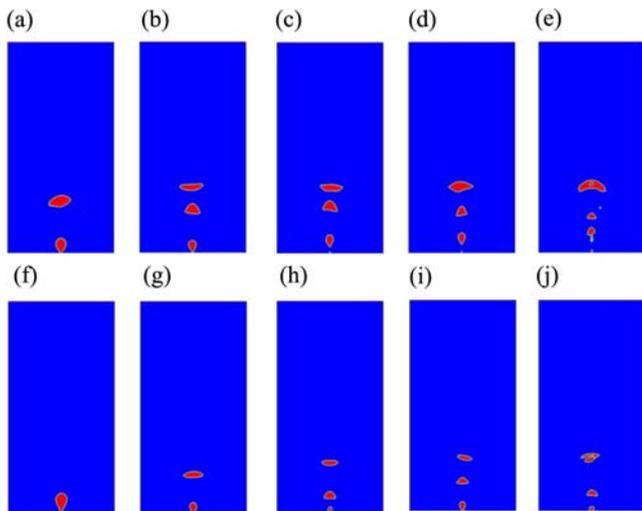
Fig. 22. Effect of liquid density on bubble behavior at constant mass flow equals to 1e-7 m³/s, (a-e) d_o=0.5 mm, (f-j) d_o=1 mm, (a, f) ρ_l=500 kg/m³, (b, g) ρ_l=998.2 kg/m³, (c, h) ρ_l=1,500 kg/m³, (d, i) ρ_l=2,000 kg/m³, (e, j) ρ_l=3,000 kg/m³.

Fig. 23. Effects of liquid density on bubble diameter when gas mass flow is 1e-7 m³/s.
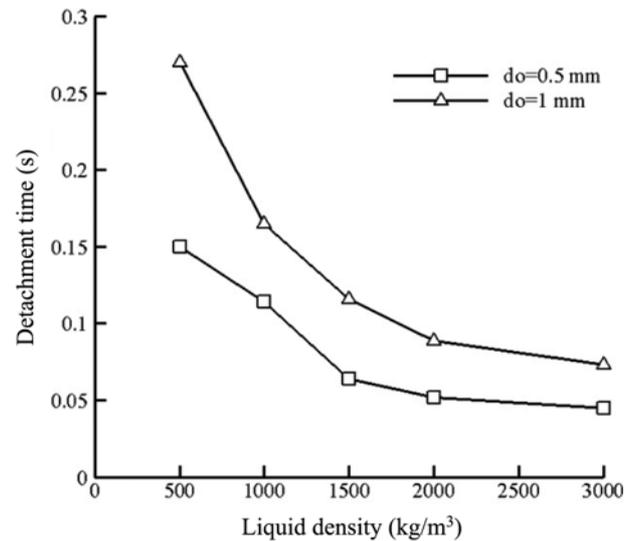
Fig. 24. Effects of liquid density on detachment time when gas mass flow is 1e-7 m³/s.

21(e); as a result, bubble formation frequency is increased by liquid density rise. The simulation results of bubbling behavior at varied liquid density when t=0.25 s and mass flow is 1e-7 m³/s are shown in Fig. 22. The effects of liquid density on diameter of bubbles and detachment time are given in Figs. 23 and 24, respectively. With the increase of liquid density at constant mass flow, bubble diameter and detachment times are reduced significantly. High liquid density results in the increase of bubble buoyancy, which can make the bubble detach early with less gas into the bubble. Therefore, average bubble diameter also decreases with the increase of liquid density.

9. Bubble Collapse Simulation at a Free Surface

Collapsing bubbles are very common phenomenon. They play an integral role in many natural as well as industrial processes (in physics, chemical and mechanical engineering, oceanography, geo-

physics, technology, and even medicine) [32]. Nevertheless, their behavior is often surprising and in many cases, still not fully understood. To simulate a spherical bubble collapse at free surface using the VOF method, we considered a mesh zone of 120×120 cells, which half of it was defined as liquid phase and the other one as gas phase. A gas phase spherical bubble with 4 mm diameter was released in liquid phase at 4mm distance of free surface. The physical model of bubble rising process is shown in Fig. 25.

At the free surface, the shape of a bubble results from a balance between two opposing effects: the buoyancy F_B, of the order of $\rho g \pi R^2$, which tends to make it emerge from the free surface and the capillary force F_C inside the hemispherical thin liquid film, of the order of $(\gamma/R)\pi R^2 = \gamma \pi R$, which tends to maintain the bubble below the surface, and γ and ρ, are, respectively, the liquid surface tension and the liquid density [32].

The radius of curvature of the emerged bubble cap is approxi-
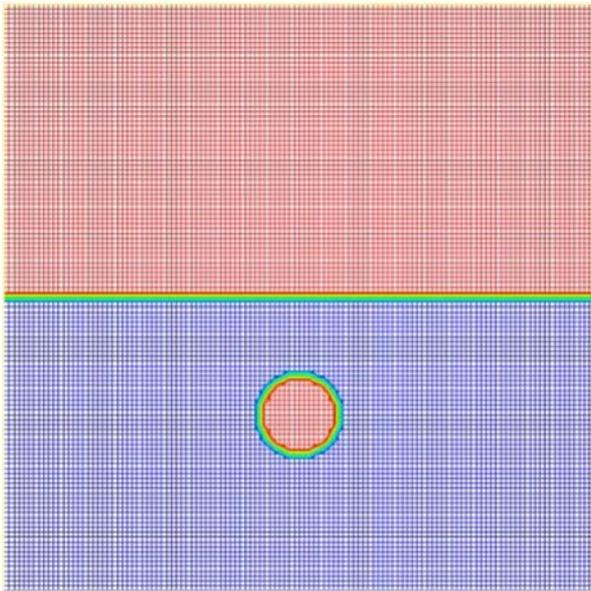
Fig. 25. Physical model of single bubble collapsing process at free surface.

mately twice that of the submerged bubble volume as it is seen in the photographic image shown in Fig. 26. At the free surface, since bubbles' radii are significantly smaller than the capillary length, the liquid films of bubble caps progressively get thinner due to capillary drainage. When the liquid film of a bubble cap reaches a critical thickness, it becomes fragile and finally ruptures. Simulated results of single bubble rising and collapsing using the volume of fluid method are given in Fig. 27. It is evident that once the bubble reaches the free surface it collapses abruptly, which is in contrast with experimental observations. As a result, we can conclude the VOF method is currently not capable of simulating a realistic bubble collapse at free surfaces and this approach should be developed further in order to simulate this process accurately.

CONCLUSION

The VOF model was used to simulate 2D bubble formation from a submerged orifice, bubble behavior and rising. The simulation results were in reasonable agreement with literature and the experiment observations captured by high-speed photograph technique. The VOF method is one of the most well known methods for volume
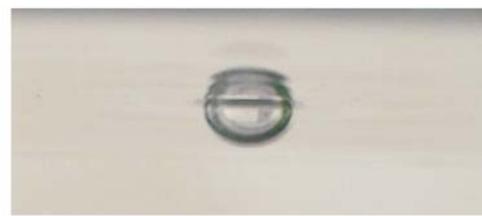
Fig. 26. Rosen bubble to free surface before collapsing.
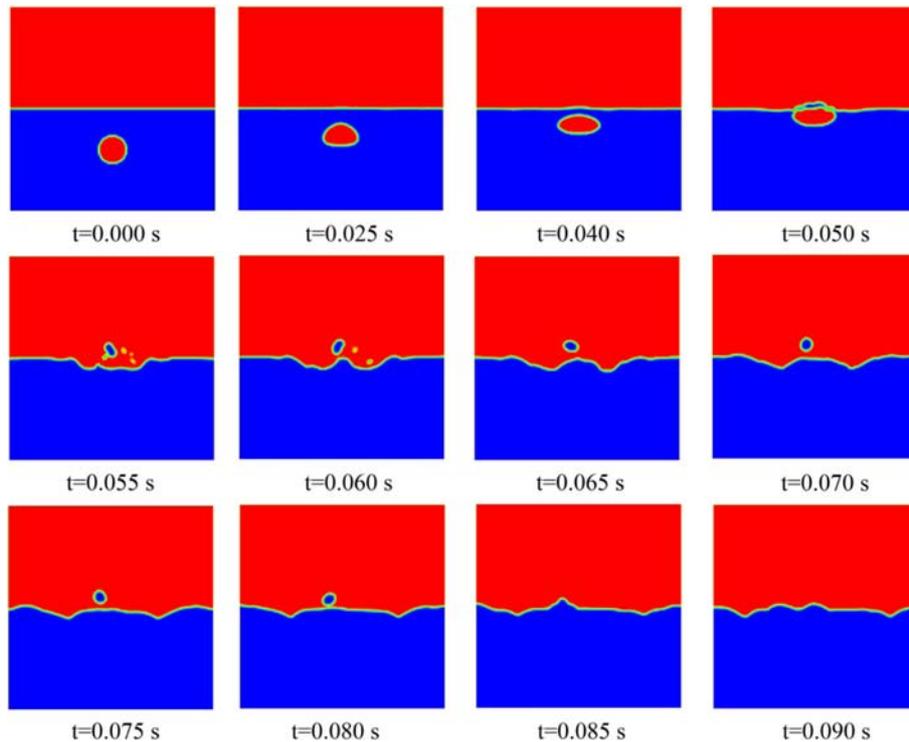
Fig. 27. Simulation of bubble collapsing at free surface.

tracking in which the motion of phases is modeled by solving a single set transport equation. The VOF method can be used to accurately predict the shape of the interface between the fluids, and in order to interface simulation of gas-liquid with deformation it is highly beneficial because of its inherent characteristics of this model in mass conservation and decrease of computational costs.

Effects of physical and geometrical properties were considered on bubble behavior. These factors are orifice diameter, surface tension, liquid density and viscosity. Bubble diameter, detachment time and bubble motion in liquid phase were investigated as well as bubble collapsing at free surface.

Simulation results indicate that the decrease in orifice diameter at constant mass flow leads to the increase of bubble diameter and the reduction of bubble formation frequency. In addition, at constant orifice diameter, increasing the surface tension was followed by bubble formation reduction and rising in bubble diameter and detachment time. Bubble diameter and detachment time grew negligibly when the liquid viscosity increased. However, results indicate that the effect of liquid viscosity on bubbling behavior is not considerable at present simulations. With the increase of liquid density at constant mass flow, bubble diameter and detachment time were reduced exponentially. In bubble collapsing simulation at free surface, it was noticeable that bubbles reached to free surface, followed by an immediate collapse, which it is in contrast with experimental observations where collapse occurs in another way and after some milliseconds reaching to the surface.

2D Simulation results were in good agreement by experimental observations, which would be beneficial in design of two-phase systems, particularly in bubble column reactors. However, there are still several limitations which should be treated in the future work. The simulations were performed in 2D Cartesian coordinates, and the 2D hydrodynamic is unrealistic in most multiphase systems. Nevertheless, the VOF model has shown its merits in simulation of multiphase flows, hence, further work is suggested in droplet behavior and boiling simulation for instance.

REFERENCES

1. N. Kantarci, F. Borak and K. O. Ulgen, *Process Biochem.*, **40**, 2263 (2005).
2. H. Li and A. Prakash, *Chem. Eng. Sci.*, **54**, 5265 (1999).
3. H. Li and A. Prakash, *Powder Technol.*, **113**, 158 (2000).
4. R. Schafer, C. Marten and G. Eigenberger, *Exp. Therm. Fluid Sci.*, **26**, 595 (2002).
5. V. V. Buwa and V. V. Ranade, *Chem. Eng. Sci.*, **57**, 4715 (2002).
6. V. Michele and D. C. Hempel, *Chem. Eng. Sci.*, **57**, 1899 (2002).
7. M. T. Dhotre, K. Ekambara and J. B. Joshi, *Exp. Therm. Fluid Sci.*, **28**, 407 (2004).
8. B. N. Thorat and J. B. Joshi, *Exp. Therm. Fluid Sci.*, **28**, 423 (2004).
9. N. Yang, J. H. Chen, W. Ge and J. H. Li, *Chem. Eng. Sci.*, **62**, 6978 (2007).
10. N. Yang, J. H. Chen, W. Ge and J. H. Li, *Chem. Eng. Sci.*, **65**, 517 (2010).
11. N. Yang, Z. Wu, J. Chen, Y. Wang and J. Li, *Chem. Eng. Sci.*, **66**, 3212 (2011).
12. D. Ma, M. Liu, Y. Zu and C. Tang, *Chem. Eng. Sci.*, **72**, 61 (2012).
13. E. Delnoij, J. A. M. Kuipers and W. P. M. van Swaaij, *Chem. Eng. Sci.*, **52**, 3623 (1997).
14. R. Krishna and J. M. van Baten, *Chem. Eng. Res. Design*, **79**, 283 (2001).
15. G. Q. Yang, B. Du and L. S. Fan, *Chem. Eng. Sci.*, **62**, 2 (2007).
16. C. W. Hirt and B. D. Nichols, *J. Comput. Phys.*, **39**, 201 (1981).
17. S. W. J. Welch and J. Wilson, *J. Comput. Phys.*, **160**, 662 (2000).
18. M. G. Wohak and H. Beer, *Numerical Heat Transfer, Part A*, **33**, 561 (1998).
19. M. R. Davidson and M. Rudman, *Numerical Heat Transfer, Part B*, **41**, 291 (2002).
20. D. J. E. Harvie and D. F. Fletcher, *Int. J. Heat Mass Transfer*, **44**, 2633 (2001).
21. D. J. E. Harvie and D. F. Fletcher, *Int. J. Heat Mass Transfer*, **44**, 2643 (2001).
22. N. Nikolopoulos, A. Theodorakakos and G. Bergeles, *Int. J. Heat Mass Transfer*, **50**, 303 (2007).
23. G. Strotos, M. Gavaises, A. Theodorakakos and G. Bergeles, *Int. J. Heat Mass Transfer*, **51**, 1516 (2008).
24. G. H. Yeoh and J. Tu, *Computational Techniques for Multiphase Flows - Basics and Applications*, Elsevier Ltd., 462 (2010).
25. N. Ashgriz and J. Y. Poo, *J. Comput. Phys.*, **93**, 449 (1991).
26. D. L. Youngs, *Time-dependent multi-material flow with large fluid distortion*, In K. W. Morton & M. J. Baines (Eds.), *Numerical methods for fluid dynamics*, London: Academic Press, 273 (1982).
27. J. U. Brackbill, D. B. Kothe and C. Zemach, *J. Comput. Phys.*, **100**, 335 (1992).
28. J. Klostermann, K. Schaake and R. Schwarze, *Int. J. Numerical Methods in Fluids*, DOI:10.1002/fld.3692.
29. E. Delnoij, J. Kuipers and W. van Swaaij, *Chem. Eng. Sci.*, **52**, 3759 (1997).
30. Z. Yujie, L. Mingyan, X. Yonggui and T. Can, *Chem. Eng. Sci.*, **73**, 55 (2012).
31. D. Bhaga and M. E. Weber, *J. Fluid Mech.*, **105**, 61 (1981).
32. G. Liger-Belair, T. Seon and A. Antkowiak, *Bubble Science, Engineering and Technology*, **4**, 21 (2012).